Mechanism of Benzene Tribopolymerization on the $RuO_2(110)$ Surface

J. Yang, Y. Qi, H. D. Kim, and A. M. Rappe*

Department of Chemistry, University of Pennsylvania, Philadelphia, Pennsylvania 19104-6323, USA

(Received 19 June 2017; revised manuscript received 25 February 2018; published 26 April 2018)

A tribopolymer formed on the contacts of microelectromechanical and nanoelectromechanical system (MEMS-NEMS) devices is a major concern hampering their practical use in information technology. Conductive metal oxides, such as RuO_2 and ReO_3, have been regarded as promising candidate materials for MEMS-NEMS contacts due to their conductivity, hardness, and relatively chemically inert surfaces. However, recent experimental works demonstrate that trace amounts of a polymer could still form on RuO_2 surfaces. We demonstrate the mechanism of this class of unexpected tribopolymer formation by conducting density-functional-theory-based computational compression experiments with benzene as the contamination gas. First, mechanical force during compression changes the benzene molecules from slightly physisorbed to strongly chemisorbed. Further compression causes deformation and chemical linkage of the benzene molecules. Finally, the two contacts detach, with one having a complex organic molecule attached and the other a more reactive surface. The complex organic molecule, which has an oxabicyclic segment, can be viewed as the rudiment of a tribopolymer, and the more reactive surface can trigger the next adsorption-reaction-tribopolymer formation cycle. Based on these results, we also predict tribopolymer formation rates by using transition-state theory and the second-order rate law. We promote a deeper understanding of tribopolymer formation (especially on metal oxides) and provide strategies for suppressing tribopolymerization.

DOI: 10.1103/PhysRevApplied.9.044038

I. INTRODUCTION

Nano- and microelectromechanical system (NEMS and MEMS) switches are potential next-generation electronic computing devices that could offer improved computational efficiency due to their small scale, low power consumption, and high speed [1–7]. Different from complementary metal-oxide-semiconductor (CMOS) transistors, the on and off states of NEMS and MEMS are modulated by the closing and opening of the contacts, which could bridge the source and drain terminals into a closed circuit. In such an operation, there is essentially no open-circuit leakage or energy dissipation. However, after some switching cycles, a tribopolymer (a kind of polymer caused by pressing and rubbing contacts together mechanically) forms on the surfaces of the contacts and severely reduces their conductivity [8]. This effect hampers the practical application of NEMS and MEMS, and therefore understanding the underlying mechanism of tribopolymer formation is an ongoing research challenge.

Tribopolymerization has been primarily studied in the context of lubricant additives; theoretical models have been developed by using both classical and quantum molecular dynamics [9–12]. Some of the essential steps in tribopolymerization involve chemical bond breaking and formation. Therefore, first-principles-based methods are a powerful tool with distinct advantages for understanding the tribopolymer formation mechanism. Our previous work based on density-functional-theory calculations [13] demonstrated that reactive metals (Pt) can adsorb contamination gas molecules onto its surface and anchor them tightly. Mechanical load during contact closure and the effect of the metal as a catalyst together trigger the polymerization reaction [13]. Generally, conductive metal oxides, especially those with oxygen terminations, have less reactive and catalytic surfaces. Contamination gas molecules are less likely to be adsorbed, let alone to undergo a reaction. However, a recent experimental work observed a trace amount of polymer formed on RuO_2 contacts, especially when the benzene concentration is high [14]. This phenomenon indicates that tribopolymer formation on conductive oxide surfaces has a different and not well-understood mechanism. In this work, we perform density-functional-theory (DFT) calculations modeling a mechanical switching cycle, which involves a closure and detachment of the contacts, and propose reaction pathways for tribopolymer formation on $RuO_2(110)$. Moreover, based on our proposed reaction path and the calculated activation energies, we provide an estimate of tribopolymer formation rates at different contaminant gas concentrations and stresses.

*rappe@sas.upenn.edu

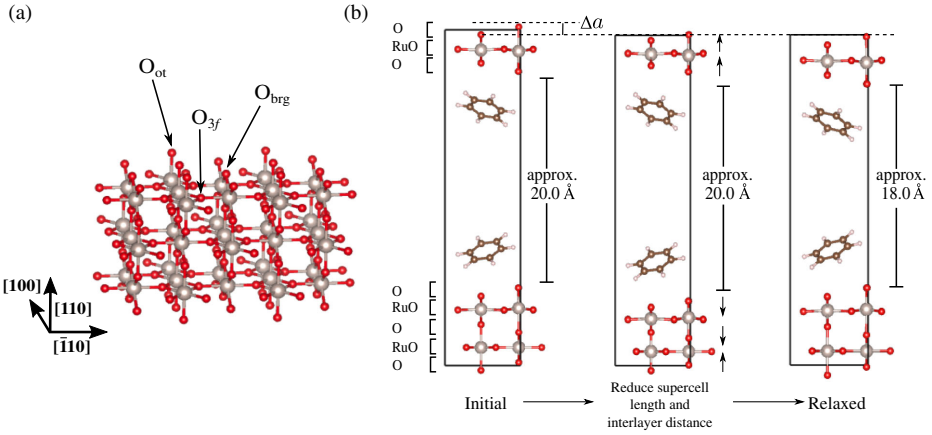

FIG. 1. Supercells for the model surface and compression analysis. (a) Ball-and-stick model of the $RuO_2(110)$-O^{cvd} surface with full oxygen coverage. The subscripts ot, $3f$, and brg refer to on-the-top, threefold-coordinated, and bridging oxygens, respectively. (b) Schematic representation of our computational compression model. The initial supercell is 30 Å long with a 20 Å vacuum space. The three–O-Ru–bilayer slab contains 11 atomic layers, judging by the location of atoms along the z direction. To simulate compression, the length of the supercell is reduced by Δa, with each interlayer distance reduced by $[(\Delta a)/(n-1)]$, where n is the number of atomic layers. The length of the center vacuum region does not change before relaxation. Oxygen atoms are in red and Ru atoms are in light gray, whereas C atoms are in brown and H atoms are in pink.

II. COMPUTATIONAL METHODS

DFT calculations are performed with the QUANTUM ESPRESSO code [15]. Norm-conserving, optimized [16], designed nonlocal [17] pseudopotentials are constructed with the OPIUM code [18] for all of the elements in the system. The exchange-correlation energy of electrons is included via the generalized-gradient-approximation density functional of Perdew, Burke, and Ernzerhof [19]. The van der Waals interaction correction is included by applying the DFTD2 method [20,21]. The kinetic-energy cutoff is 680 eV. The self-consistent relaxation calculations are converged to a total force threshold of 5 meV/Å. For the bulk structure, an $8\times8\times8$ Monkhorst-Pack mesh of k points is used. The optimized lattice parameters of RuO_2 ($P42/mnm$) are $a=b=4.4681$ Å, $c=3.0832$ Å and $\alpha=90.0°$; the lattice parameters agree with the experimental values $a=b=4.4919$ Å, $c=3.1066$ Å and $\alpha=90.0°$ [22], with an error of 0.53% in the a and b directions and 0.75% in the c direction.

For the surface model of the metal oxides, we use symmetric slabs for the $RuO_2(110)$-O^{cvd} surface, as shown in Fig. 1(a), since such a surface is the most stable case under experimental conditions [23,24]. The superscript cvd in $RuO_2(110)$-O^{cvd} refers to a fully oxygen-"covered" surface. The surface structure contains three rutile (RuO)-O bilayers capped with O. Benzene is chosen as the background contamination gas, since it comes from NEMS packaging and causes the most severe contamination [25]. The surface is fully relaxed with a 20 Å vacuum space between slabs, and an $8\times8\times1$ k-point grid is used to integrate the Brillouin zone.

In order to apply normal stress in simulations, we perform multiple steps of structural relaxation on the supercell, successively reducing the z-direction cell length. For each step of relaxation, we reduce the supercell height and the interlayer distances of the metal-oxide slab. As shown in Fig. 1(b), we keep the vacuum space fixed at the beginning and reduce each atomic interlayer spacing in the RuO_2 slab by $\Delta a=0.02$ Å. Here, we construct the slab with 11 layers of atoms, so the unit cell is reduced by 0.2 Å from the previous supercell. After relaxation, the strong Ru—O bonds tend to recover to their original interlayer distances, and the vacuum space decreases due to pressure from this interlayer expansion. As a result, the contamination gas molecules in the vacuum space sense the mechanical load along the same direction. Note that each relaxation step takes the end structure of the previous step as the starting point and utilizes atomic wave functions as the starting wave functions.

After acquiring the reaction path from the compression computational experiments, the activation energy is computed with the nudged-elastic-band (NEB) method to estimate the polymerization rates [26,27].

III. COMPUTATIONAL MECHANICAL CYCLE

To search all of the possible reaction paths, we start with two different initial benzene registries, which are referred to as full overlap and nonoverlap, respectively, as shown in Fig. 2. Computational mechanical switching cycles for both registries is also shown in Fig. 2. The supercell height is compressed down to 14 Å, which is 53% of the original cell height, and this height range (30 Å → 14 Å) is considered to be large enough to demonstrate crucial steps of tribo-polymerization. During the compression from $c=30$ Å to $c=14$ Å, benzene molecules in the two registries behave approximately the same. Upon compression from $c=30$ Å to $c=14.6$ Å, the molecules rotate and slide due to the intermolecular repulsion, and they finally become approximately parallel to the surface. Upon further

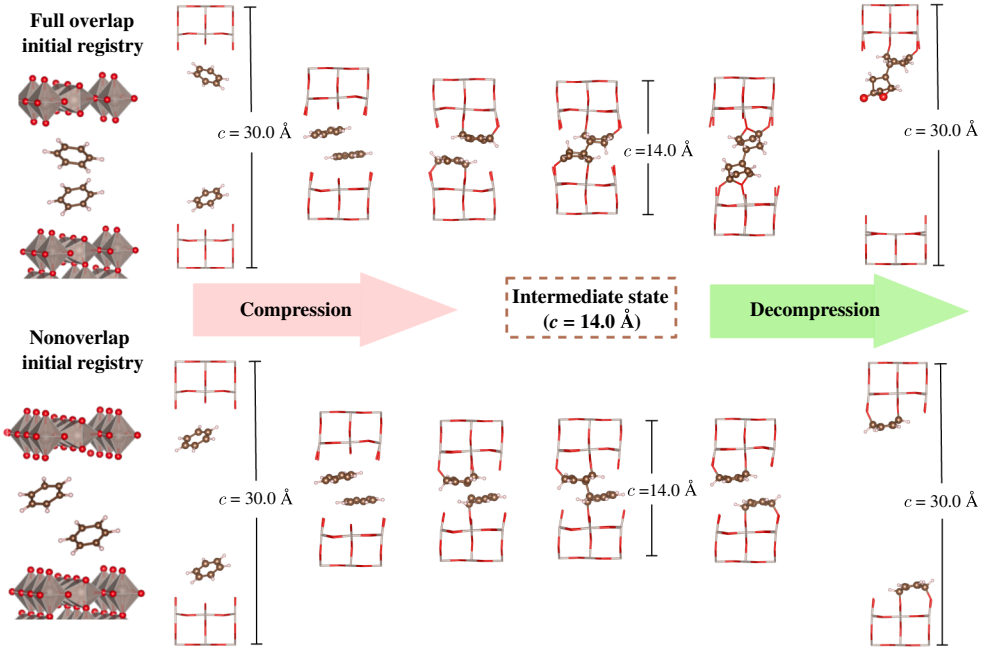

FIG. 2. Schematic picture demonstrating a mechanical cycling, which involves a compression and an expansion process. (Upper panel) The full-overlap case, in which the upper and lower benzene molecules are mirror images of each other. (Lower panel) The nonoverlap case, in which there is no overlap between the two benzene molecules. On the left of both the upper and lower panels, a $2 \times 2 \times 1$ supercell is shown for describing two initial benzene adsorption registries on the $RuO_2(110)$-O^{cvd} surface. Only the nearest layers to the molecules are shown. The supercell length ranges between 30.0 and 14.0 Å. Compression and expansion have the same step-size change. In each step, the change of the supercell length is 2 Å between $c = 30.0$ Å and $c = 18.0$ Å. This change is reduced to 0.2 Å for $15.0 < c < 16.0$ Å and further reduced to 0.1 Å when $c < 15.0$ Å, in order to have a more detailed observation of the reaction. Note that the RuO_2 surface slab is shown in stick style, with red representing O atoms and gray Ru atoms.

compression ($c = 14.6$ Å to $c = 14.0$ Å), the originally physisorbed benzene molecules begin to chemically bond with surface oxygen atoms.

As the cell length is further compressed below 14.6 Å, the two benzene molecules dimerize by forming a C—C bond. The structure of this intermediate state formed by the linkage of two benzene molecules varies with the initial registry. For a compression cycle starting with a full-overlap registry, there are hydrogen atom migrations between the bottom and the top benzene molecules, as shown in Fig. 3(a). For the

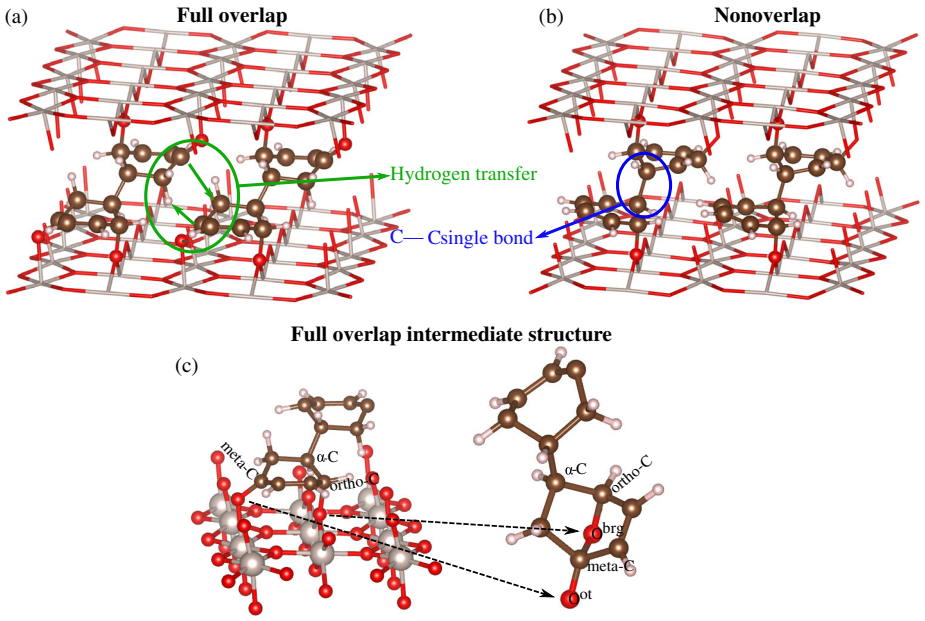

FIG. 3. Ball-and-stick model showing different intermediate-state structures. For clarity, we use thin lines to represent the RuO_2 substrate. (a) Intermediate state with H migrations. The green arrows show the hydrogen atom migrations between bottom and upper benzenes. (b) Intermediate state without H migrations. Only a C—C bond forms between the upper and lower benzenes, as shown in the blue circle. (c) The intermediate state molecule (left) and its structural change (right) during a mechanical cycling. The carbon atom connecting the upper and lower benzenes is labeled α-C. The ortho-C attaches to O^{brg}, and the meta-C attaches to O^{ot}.

nonoverlap initial registry compression, no such H atom migrations are observed during the intermediate-state formation, as shown in Fig. 3(b).

Furthermore, the decompression process ($c = 14$ Å to $c = 30$ Å) demonstrates two different phenomena after the formation of the intermediate structure. We find that, during the expansion, the intermediate biphenyl-like structure will either split into two adsorbed benzene molecules or become a biphenyl-like structure with an oxanorbornadiene segment, depending on its structure. For the intermediate state with H migrations [whose structural evolution and denomination of atoms are shown in detail in Fig. 3(c)], the two O atoms which bond with ortho-C and meta-C are extracted from the substrate. The O^{brg} atom attached to ortho-C originally also bonds to the meta-C atom, transforming the lower benzene ring into an oxanorbornadiene segment. This oxidized biphenyl-like molecule demonstrates that benzene molecules react under stress to form a complex polymeric precursor, which is the rudiment of a tribopolymer. Tribopolymer formation, therefore, involves a chain reaction of this molecule linkage process. H migration, during the formation of the intermediate state, plays an important role in inducing an O extraction reaction. After H atoms migrate away from ortho-C and meta-C, these two carbon atoms share more electrons and form stronger chemical bonds with the surface O atoms, thereby weakening the chemical bonds between the O atoms and the RuO_2 substrate. As a result, during expansion, two O atoms are extracted from the surface and an oxanorbornadiene segment forms. For an intermediate state without H migrations, the biphenyl-like structure splits into two strongly chemisorbed benzene molecules, which could also lead to further polymerization as more cycles are applied. Since the polymerization process for strongly chemisorbed molecules was well studied in our previous work [13], we do not discuss it further here.

IV. CHEMICAL KINETICS

We now focus on the case in which an oxidized biphenyl-like molecule is produced and estimate the timescale of tribopolymerization. This reaction involves two steps. First, the benzene molecules change from weakly physisorbed gas moelcules, which interact with the contacts by weak Van der Waals interaction, to strongly chemisorbed adsorbates,

$$C_6H_{6(g)} \rightarrow C_6H_{6(ads)}, \tag{1}$$

and then two chemically adsorbed benzene molecules follow a second-order reaction,

$$2C_6H_{6(ads)} \rightarrow C_{12}H_{12(ads)}. \tag{2}$$

Gas chemisorption depends on the partial pressure and the chemisorption energy. We consider the simplest relationship, the Langmuir isotherm, between the benzene molecule surface coverage, θ, and the benzene pressure, $p_{C_6H_6}$, as follows:

$$\theta_0 = \frac{p_{C_6H_6}}{p_{C_6H_6} + p_0}, \tag{3}$$

where θ_0 represents the initial equilibrium coverage, $p_{C_6H_6}$ is the initial partial pressure of benzene in the gas phase, and p_0 takes the form

$$p_0 = \left(\frac{2\pi m k_B T}{h^2}\right)^{1/2} k_B T \exp\left(-\frac{E_{ads}}{k_B T}\right). \tag{4}$$

Here, m is the molecular weight of benzene, k_B is the Boltzmann constant, T is the temperature, h is Planck's constant, and E_{ads} is the adsorption energy of benzene on the surface. The rate constant, k, for the intermediate-state formation [Eq. (2)], treated by transition state theory, can be written as

$$k = \frac{k_B T}{h} \exp\left(-\frac{\Delta E(\sigma)}{k_B T}\right), \tag{5}$$

where ΔE is the activation energy under the applied normal stress, σ. Since Eq. (2) is a second-order reaction, the rate law can be written as

$$\text{rate} = -\frac{d\theta(t)}{dt} = 2k\theta(t)^2, \tag{6}$$

where θ is the surface coverage of adsorbed benzene and k is the rate constant.

Here, we introduce the reaction half-life time ($t_{1/2}$), which is defined as the time that half of the surface adsorbates are consumed for tribopolymerization. $t_{1/2}$ is expressed as

$$t_{1/2} = \frac{1}{2k\theta_0}. \tag{7}$$

To acquire k, we calculate $\Delta E(\sigma)$ at different supercell lengths with the NEB method, as shown in Fig. 4(a). We observe that the activation energy is lower for a smaller supercell. Normal stress vs supercell length is also plotted. During the compression, the normal stress increases linearly and plateaus around 15.0 GPa. Further compression causes the normal stress drop to 11.66 GPa, indicating that the molecule-linkage reaction occurs. This stress, 15.0 GPa, is the threshold for a zero-barrier reaction, above which a polymerization reaction will occur spontaneously. This value (15.0 GPa) is also consistent with the estimated stress in experiments [28,29].

By using Eqs. (5) and (7), we calculate the reaction rate constant k and the corresponding reaction half-life at different benzene partial pressures and apply normal stresses, as

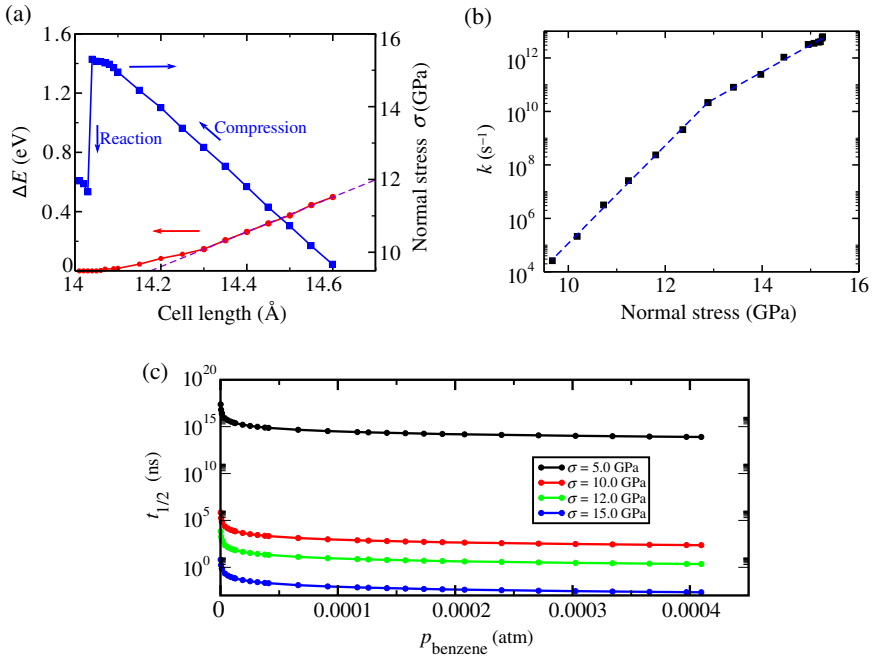

FIG. 4. (a) The activation energy (the red dots) and normal stress (the blue squares) vs the supercell length. The purple dashed line is the linear fit of the activation energy. (b) Calculated normal-stress-dependent reaction rates. The threshold stress for a zero-barrier reaction change is 15 GPa. The blue dashed lines are the linear fits. (c) Reaction half-life under different benzene partial pressures and normal stresses.

shown in Figs. 4(b) and 4(c). Smaller applied stresses and contamination gas molecule partial pressures lead to slower tribopolymer formation. The half-life decreases exponentially with benzene partial pressure, and plateaus at and above 1×10^{-4} atm, indicating the saturation of surface adsorption sites. Normal stress, which could affect the half-life by several orders of magnitude, is more influential than partial pressure. Therefore, techniques for reducing normal mechanical load, such as controlling the momentum of NEMS contacts and fabricating flatter contact surfaces (high spots on the surfaces may cause the stress to peak there) are of great significance.

V. CONCLUSION

In this paper, we carry out DFT calculations to reveal the tribopolymer formation mechanism on the $RuO_2(110)$-O^{cvd} surface. We find that normal stress changes molecular adsorption from weak physisorption to strong chemisorption, and sufficient stress (15 GPa) causes benzene molecules to link to form an intermediate biphenyl-like state, which can adopt two different structures. One, with H migration, changes to a biphenyl-like molecule with an oxabicyclic segment, which is the rudiment of a tribopolymer. Another structure, without H migration, splits into two adsorbed benzene molecules. Furthermore, we predict the reaction rates based on the transition-state theory and the second-order rate law. This work provides more insight into the mechanochemical reactions of tribopolymerization on conductive oxides.

ACKNOWLEDGMENTS

J. Y. was supported by the U.S. National Science Foundation under Grant No. CMMI-1334241. H. D. K. was supported by the University of Pennsylvania NSF/Louis Stokes Alliance for Minority Participation (LSAMP) program. Y. Q. was supported by the U.S. National Science Foundation under Grant No. DMR-1124696. A. M. R. was supported by the U.S. Department of Energy under Grant No. DE-FG02-07ER15920. Computational support was provided by the High Performance Computing Modernization Program of the Department of Defense and the National Energy Research Scientific Computing Center of the Department of Energy.

[1] T.-J. K. Liu, D. Markovic, V. Stojanović, and E. Alon, The relay reborn, IEEE Spectrum **49**, 40 (2012).
[2] M. Spencer, F. Chen, C. C. Wang, R. Nathanael, H. Fariborzi, A. Gupta, H. Kam, V. Pott, J. Jeon, T.-J. K. Liu, D. Markovć, E. Alon, and V. Stojanović, Demonstration of integrated micro-electro-mechanical relay circuits for VLSI applications, IEEE J. Solid-State Circuits **46**, 308 (2011).
[3] O. Y. Loh and H. D. Espinosa, Nanoelectromechanical contact switches, Nat. Nanotechnol. **7**, 283 (2012).
[4] Y. J. Kim and W. Y. Choi, Nonvolatile nanoelectromechanical memory switches for low-power and high-speed field-programmable gate arrays, IEEE Trans. Electron Devices **62**, 673 (2015).
[5] Y.-H. Yoon, Y.-H. Song, S.-D. Ko, C.-H. Han, G.-S. Yun, M.-H. Seo, and J.-B. Yoon, A highly reliable MEMS relay with two-step spring system and heat sink insulator for power applications, J. Microelectromech. Syst. **25**, 217 (2015).
[6] J. Yeon, X. He, A. Martini, and S. H. Kim, Mechanochemistry at solid surfaces: Polymerization of adsorbed molecules by mechanical shear at tribological interfaces, ACS Appl. Mater. Interfaces **9**, 3142 (2017).
[7] Z. Ye, A. Martini, P. Thiel, H. H. Lovelady, K. McLaughlin, and D. A. Rabson, Atomistic simulation of frictional

anisotropy on quasicrystal approximant surfaces, Phys. Rev. B **93**, 235438 (2016).

[8] F. Streller, G. E. Wabiszewski, F. Mangolini, G. Feng, and R. W. Carpick, Tunable, source-controlled formation of platinum silicides and nanogaps from thin precursor films, Adv. Mater. Interfaces **1**, 1300120 (2014).

[9] M. J. Furey, C. Kajdas, G. J. Molina, and B. A. Vick, Critical assessment of tribopolymerization as an antiwear mechanism, in *Proceedings of World Tribology Congress III, Washington, DC, 2005* (American Society of Mechanical Engineers, New York, 2005), p. 621.

[10] C. Minfray, T. Le Mogne, J.-M. Martin, T. Onodera, S. Nara, S. Takahashi, H. Tsuboi, M. Koyama, A. Endou, H. Takaba, M. Kubo, C. A. Del Carpio, and A. Miyamoto, Experimental and molecular dynamics simulations of tribochemical reactions with ZDDP: Zinc phosphate-iron oxide reaction, Tribol. Trans. **51**, 589 (2008).

[11] T. Onodera, R. Miura, A. Suzuki, H. Tsuboi, N. Hatakeyama, A. Endou, H. Takaba, M. Kubo, and A. Miyamoto, Development of a quantum chemical molecular dynamics tribochemical simulator and its application to tribochemical reaction dynamics of lubricant additives, Model. Simul. Mater. Sci. Eng. **18**, 034009 (2010).

[12] M. Koyama, J. Hayakawa, T. Onodera, K. Ito, H. Tsuboi, A. Endou, M. Kubo, C. A. Del Carpio, and A. Miyamoto, Tribochemical reaction dynamics of phosphoric ester lubricant additive by using a hybrid tight-binding quantum chemical molecular dynamics method, J. Phys. Chem. B **110**, 17507 (2006).

[13] Y. Qi, J. Yang, and A. M. Rappe, Theoretical modeling of tribochemical reaction on Pt and Au contacts: Mechanical load and catalysis, ACS Appl. Mater. Interfaces **8**, 7529 (2016).

[14] V. Brand, M. S. Baker, and M. P. de Boer, Contamination thresholds of Pt- and RuO_2-coated Ohmic switches, J. Microelectromech. Syst. **22**, 1248 (2013).

[15] P. Giannozzi *et al.*, QUANTUM ESPRESSO: A modular and open-source software project for quantum simulations of materials, J. Phys. Condens. Matter **21**, 395502 (2009).

[16] A. M. Rappe, K. M. Rabe, E. Kaxiras, and J. D. Joannopoulos, Optimized pseudopotentials, Phys. Rev. B **41**, 1227(R) (1990).

[17] N. J. Ramer and A. M. Rappe, Designed nonlocal pseudopotentials for enhanced transferability, Phys. Rev. B **59**, 12471 (1999).

[18] See http://opium.sourceforge.net.

[19] J. P. Perdew, K. Burke, and M. Ernzerhof, Generalized Gradient Approximation Made Simple, Phys. Rev. Lett. **77**, 3865 (1996).

[20] S. Grimme, Semiempirical GGA-type density functional constructed with a long-range dispersion correction, J. Comput. Chem. **27**, 1787 (2006).

[21] V. Barone, M. Casarin, D. Forrer, M. Pavone, M. Sambi, and A. Vittadini, Role and effective treatment of dispersive forces in materials: Polyethylene and graphite crystals as test cases, J. Comput. Chem. **30**, 934 (2009).

[22] C.-E. Boman, Refinement of the crystal structure of ruthenium dioxide, Acta Chem. Scand. **24**, 116 (1970).

[23] K. Reuter and M. Scheffler, Composition, structure, and stability of $RuO_2(110)$ as a function of oxygen pressure, Phys. Rev. B **65**, 035406 (2001).

[24] H.-S. D. Kim, J. Yang, Y. Qi, and A. M. Rappe, Adsorption of benzene on the $RuO_2(110)$ surface, J. Phys. Chem. C **121**, 1585 (2017).

[25] H. W. Hermance and T. F. Egan, Organic deposits on precious metal contacts, Bell Syst. Tech. J. **37**, 739 (1958).

[26] G. Henkelman and H. Jónsson, Long time scale kinetic Monte Carlo simulations without lattice approximation and predefined event table, J. Chem. Phys. **115**, 9657 (2001).

[27] G. Henkelman, B. P. Uberuaga, and H. Jónsson, A climbing image nudged elastic band method for finding saddle points and minimum energy paths, J. Chem. Phys. **113**, 9901 (2000).

[28] J. Zhu, K. B. Yeap, K. Zeng, and Li Lu, Nanomechanical characterization of sputtered RuO_2 thin film on silicon substrate for solid state electronic devices, Thin Solid Films **519**, 1914 (2011).

[29] V. Brand, M. S. Baker, and M. P. de Boer, Impact of contact materials and operating conditions on stability of micromechanical switches, Tribol. Lett. **51**, 341 (2013).